Physica Scripta

INCLUSIVE PUBLISHING TRUSTED SCIENCE

PURPOSE-LED PUBLISHING™

PAPER • **OPEN ACCESS**

The structural, magnetic, electronic, optical and mechanical properties of some rare earth sesquioxides Re_2O_3 (Re = Gd and Tb): first-principles calculations

To cite this article: Sedat Durman and Sevket Simsek 2026 *Phys. Scr.* **101** 325902

View the article online for updates and enhancements.

You may also like

- Band structures of RE_2O_3:Eu (RE = Lu, Y, Sc) from perspective of spin-polarized quasi-particle approximation
ShiJie Chen, Yaoping Xie, He Feng et al.
- Electric field gradients of ^{111}Cd in monoclinic (B-phase) rare earth sesquioxides
D Lupascu, M Uhrmacher and K P Lieb
- Phononic origin of the infrared dielectric properties of RE_2O_3 (RE = Y, Gd, Ho, Lu) compounds
Yixiu Luo, Juan Wang, Luchao Sun et al.

This content was downloaded from IP address 95.183.140.37 on 29/08/2026 at 22:03

Physica Scripta

Check for updates

OPEN ACCESS

RECEIVED
20 April 2026

REVISED
11 July 2026

ACCEPTED FOR PUBLICATION
27 July 2026

PUBLISHED
6 August 2026

Original content from this work may be used under the terms of the Creative Commons Attribution 4.0 licence.

Any further distribution of this work must maintain attribution to the author(s) and the title of the work, journal citation and DOI.

PAPER

The structural, magnetic, electronic, optical and mechanical properties of some rare earth sesquioxides Re_2O_3 (Re = Gd and Tb): first-principles calculations

Sedat Durman and Sevket Simsek*

Department of Material Science and Engineering, Faculty of Engineering, Hakkari University, Hakkari 30000, Türkiye
* Author to whom any correspondence should be addressed

E-mail: ssimsek@hakkari.edu.tr and sedatdurman401722@gmail.com

Keywords: Gd_2O_3, Tb_2O_3, rare earth sesquioxides, first-principles calculations, electronic structure, optical, elastic properties

Abstract

This work presents a comprehensive study on the physical properties of A-type Re_2O_3 (Re = Gd, Tb) rare earth sesquioxides. The structural, magnetic, electronic, optical and mechanical properties of Gd_2O_3 and Tb_2O_3 sesquioxides were investigated using different theoretical approaches such as GGA-PBEsol (the Perdew-Burke-Ernzerhof functional tuned in particular for properties of solids), mbjLDA, HSE06 and GGA + U_{eff} based on density functional theory. Structural optimisations of the compounds under consideration were conducted utilising the GGA-PBEsol and HSE06 method and the findings show that they are in good agreement with the results in the literature. GGA-PBEsol, mbjLDA and HSE06 methods were utilised to accurately analyse the electronic properties of both compounds and the results demonstrate that both compounds are magnetic insulator materials with indirect band gap (Γ–K). Additionally, the results obtained with the GGA + U_{eff} method also confirm that both compounds have indirect band gaps. The calculated magnetic moment of Gd and Tb atoms is found to be 6.926 μB and 5.916 μB, respectively. On the other hand, the frequency dependent dielectric function of Gd_2O_3 and Tb_2O_3 compounds was calculated for their potential applications in optical materials and the obtained results show that both compounds may be suitable for ultraviolet optoelectronic applications. From the calculated elastic constants, Gd_2O_3 and Tb_2O_3 compounds were predicted to be mechanically stable, ductile and soft materials.

1. Introduction

Rare earth elements (Re) and their sesquioxides (Re_2O_3) have recently become some of the most scientifically and technologically interesting materials due to their critical importance in many fields, from nuclear power reactors to lasers, from medical imaging to optoelectronic devices. Rare earth sesquioxides have potential applications in many fields, including magnetic cooling, magnetic resonance imaging (MRI), light emitters, ultra-fast lasers, optical biosensors, and nuclear energy [1–5]. These compounds are known to exhibit five different polymorphic structures, depending on the radius of the rare earth cations (Re^{3+}) and the temperature. Rare earth sesquioxides manifest in two phases at temperatures above 2273 K, called X-type (cubic, space group *Im*-3 *m*) and H-type (hexagonal, space group *P*63/*mmc*), while at temperatures below 2273 K they exist in three phases, namely C-type (cubic phase, space group *Ia*-3), B-type (monoclinic phase, space group *C*2/*m*) and A-type (hexagonal phase, space group *P*-3*m*1) [6]. The compounds gadolinium oxide (Gd_2O_3) and terbium oxide (Tb_2O_3) also belong to the rare earth sesquioxide family. Gd_2O_3 is utilised as a contrast agent in the field of medical MRI due to its paramagnetic properties [2], and as a burnable absorber material in nuclear reactors to enhance the reactivity of the reactor due to its high neutron absorption cross section [7]. While it is preferred in complementary metal-oxide-semiconductor technology due to its high dielectric constant [8], it is used as a thermal barrier coating in gas turbine engines due to its high melting point and low thermal

© 2026 The Author(s). Published by IOP Publishing Ltd

conductivity [4]. The high thermodynamic stability and refractive index of these crystals makes them well suited to a variety of optical applications, including corrosion-resistant coatings, anti-reflective coatings, modulators and optical filters [9]. Moreover, the low phonon energy of Gd_2O_3 renders it a suitable host for the luminescence of rare earth ions. When doped with rare earth ions such as Er^{3+}, Tb^{3+}, Yb^{3+} and Eu^{3+}, the luminescence properties are significantly increased [10, 11]. On the other hand, thanks to its high Verdet constant, Tb_2O_3 is one of the most preferred materials in magneto-optical systems. It has been reported to have a Verdet constant approximately 3.5 times greater than that of commercial $Tb_3Ga_5O_{12}$ (TGG) single crystals [12–14]. This makes it a prime candidate for use in Faraday isolators (FIs) and rotators.

A comprehensive understanding of the physical properties of Gd_2O_3 and Tb_2O_3 sesquioxides is of great scientific and technological importance. These compounds exhibit interesting electronic and optical properties, which can be attributed to the 4 f electrons present in their structure. There are numerous studies in the literature on the structural phase transitions, luminescence properties, and magneto-optical properties of Gd_2O_3 and Tb_2O_3 compounds. However, to the best of our knowledge, there is no comprehensive study of the structural, electronic, optical, and elastic properties of A-type (hexagonal) Gd_2O_3 and Tb_2O_3 compounds. The aim of this study is to comprehensively investigate the physical properties of hexagonal Gd_2O_3 and Tb_2O_3 compounds using density functional theory (DFT). For this purpose, the electronic, optical, magnetic, and elastic properties of both compounds were comprehensively addressed using the GGA-PBEsol (the Perdew-Burke-Ernzerhof functional tuned in particular for properties of solids), mbjLDA, and HSE06 functionals. Additionally, due to the strong correlation between f electrons of Gd and Tb atoms, the electronic, optical, magnetic and elastic properties of both compounds were re-evaluated under the GGA + U approach. The results obtained are expected to provide valuable insights into the theoretical and experimental studies on Gd_2O_3 and Tb_2O_3.

2. Calculation method

All calculations in this study were performed with MedeA Vienna *ab initio* simulation package (VASP), utilising the *ab initio* total energy and molecular dynamics package VASP [15, 16]. The exchange and correlation energy between electrons was treated with the GGA-PBEsol [17], mbjLDA (the Tran-Blaha modified Becke-Johnson potential) [18] and HSE06 functionals (the hybrid Heyd–Scuseria–Ernzerhof functionals) [19]. The projector augmented wave method [20] was employed for Re_2O_3 compounds, with an energy cut-off set at 600 eV. The crystal structures of both compounds were optimised by the GGA-PBEsol and HSE06 functionals using convergence criteria of 10^{-7} eV for the electronic iterations and 0.01 eV $Å^{-1}$ for the ionic relaxations. In order to enhance comprehension of the electronic and optical properties of Re_2O_3 compounds, the electronic band structure and optical properties were calculated using three different approaches, including GGA-PBEsol, mbjLDA and HSE06. The elastic properties of the compounds under consideration were calculated by means of the strain–stress method with 0.01 strain using the GGA-PBEsol and HSE06 functionals, as implemented in the MedeA VASP [21–23]. On the other hand, due to the strong correlation between the localized f electrons of Gd and Tb atoms, the GGA + U approach proposed by Liechtenstein [24] was also utilized to investigate the structural, electronic, optical, and elastic properties of the Gd_2O_3 and Tb_2O_3 compounds. In this approach, the on-site Coulomb interaction (U) and the exchange interaction (J) are combined into a single effective Hubbard parameter, defined as $U_{\text{eff}} = U—J$ [24]. To ensure consistency, this parameter is referred to as U_{eff} throughout the entire manuscript. In addition, to avoid high computational costs and to focus primarily on the comparative performance of the GGA-PBEsol, mbjLDA, HSE06 and GGA + U_{eff} schemes, spin–orbit coupling was not included.

3. Results

3.1. Structural and magnetic properties

The rare earth sesquioxides Gd_2O_3 and Tb_2O_3 crystallize in A-type hexagonal phase with the space group *P*-3*m1* (#164). In Re_2O_3 (Re = Gd and Tb) compounds, two Re atoms were located at the 2d Wyckoff site (1/3, 2/3, z), while the O_1 and O_2 atoms were positioned at the 2d Wyckoff site (1/3, 2/3, z) and at the 1a Wyckoff site (0.0, 0.0, 0.0), respectively. To determine the magnetic ground states of the Gd_2O_3 and Tb_2O_3 compounds in A-type hexagonal phase, the total energies corresponding to the ferromagnetic (FM) and antiferromagnetic (AFM) states were calculated and analysed by considering the energy difference between them ($\Delta E = E_{\text{AFM}} - E_{\text{FM}}$). The variation of ΔE as a function of U_{eff},

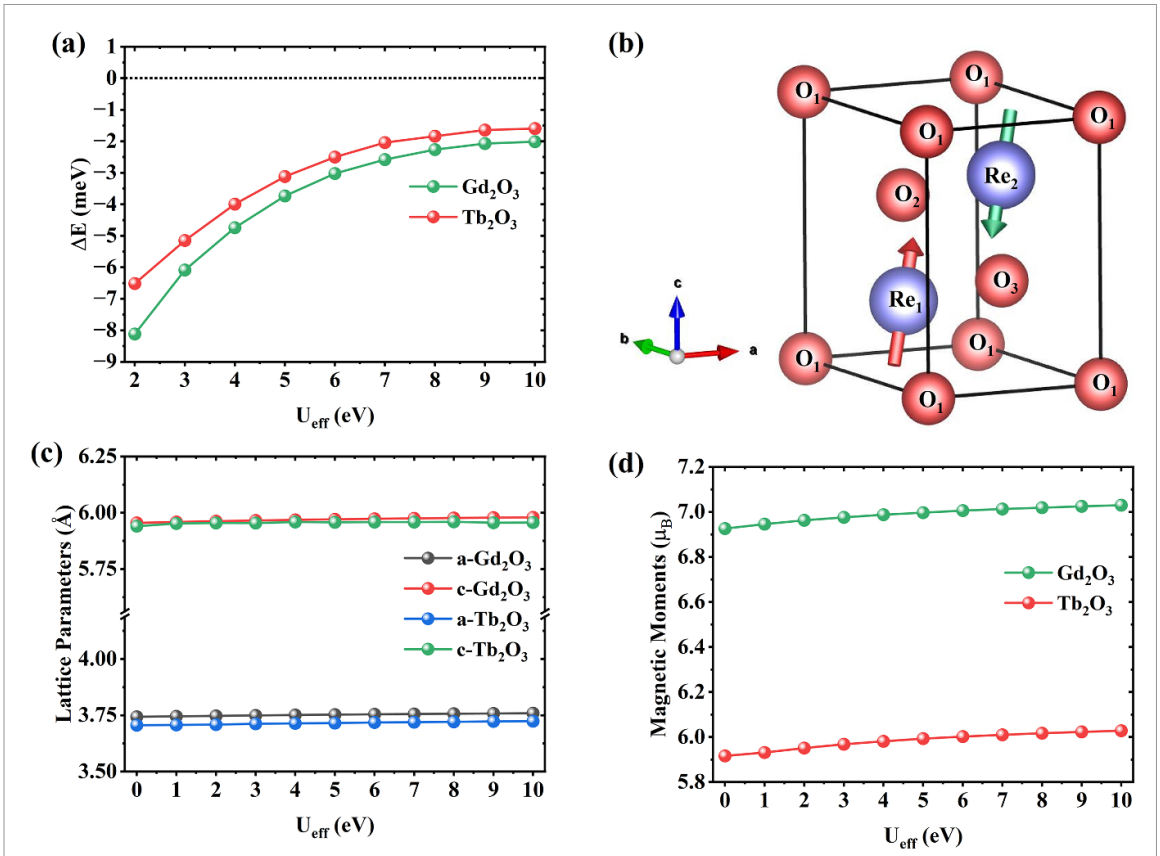


Figure 1. Calculated (a) energy difference between antiferromagnetic (AFM) and ferromagnetic (FM) spin ordering ($\Delta E = E_{AFM} - E_{FM}$), (b) the unit cell of trigonal Re_2O_3 (A-type hexagonal phase, space group *P*-3*m*1) in an AFM spin arrangement, (c) lattice parameters and (d) magnetic moments of Re_2O_3 sesquioxides as a function of U_{eff}.

presented in figure 1(a), reveals that ΔE is negative for all U_{eff} values. These results suggest that both compounds favour the AFM ground state, which is energetically more stable. Therefore, all subsequent calculations were performed considering the AFM ground state for both compounds. The unit cell of trigonal Re_2O_3 in the AFM spin arrangement was constructed using VESTA [25] and is presented in figure 1(b). In order to obtain the fully relaxed structure of both compounds, both ionic positions and lattice geometries were optimised using GGA-PBEsol and HSE06 functionals, and the results are presented in table 1. The obtained lattice constants are found to be in agreement with both theoretical and experimental values. The effects of the effective Hubbard parameter (U_{eff}) on the lattice constants in the GGA + U_{eff} approximation for Re_2O_3 compounds were investigated. The variation of the lattice parameters with U_{eff} from 1 eV to 10 eV for both compounds is shown in figure 1(c). The lattice parameters of both compounds demonstrate very small changes with increasing U_{eff}, as illustrated in figure 1(c). On the other hand, the magnetic moments of the Gd and Tb atoms were calculated as a function of U_{eff} and are shown in figure 1(d). When $U_{eff} = 0$, the magnetic moments of the Gd and Tb atoms were found to be 6.926 μB and 5.916 μB, respectively. As can be seen in figure 1(d), the magnetic moments of both atoms increase as U_{eff} increases. These results demonstrate that, while the U_{eff} term has a negligible impact on the lattice parameters of both compounds, it noteworthily influences the magnetic moments of the Gd and Tb atoms.

3.2. Electronic properties

The accurate determination of the electronic structure of a material is technologically very important. The exchange and correlation energy are critical for the accurate prediction of the forbidden band gaps of semiconductors and insulators. In DFT calculations, a variety of approaches are employed for the identification of exchange and correlation energy, including LDA, GGA, mbjLDA and HSE06 functionals. Furthermore, for systems with d and f electrons, the GGA + U_{eff} approach is utilised to accurately describe the interaction between electrons. The electronic band structure and density of states (DOS) of Gd_2O_3 and Tb_2O_3 compounds were calculated using GGA-PBEsol, mbjLDA and HSE06 functionals as well as GGA + U_{eff} approaches. For A-type hexagonal Re_2O_3 sesquioxides shown in figure 1(b), the high-symmetry points of the Brillouin zone used in this study are Γ (0, 0, 0), *M* (1/2, 0, 0), *K* (1/3, 1/3,

Table 1. The calculated lattice parameters and band gaps of Gd_2O_3 and Tb_2O_3.

Material	References	$a = b$ (Å)	c (Å)	E_g (eV)
Gd_2O_3	GGA-PBEsol$^{cal.}$	3.691	5.802	4.04
	HSE06^{cal}	3.689	5.849	5.61
	mbjLDA^{cal}	—	—	5.86
	GGA-PBE [26]	3.730	5.938	—
	GGA-PBE [27]	3.80	5.95	—
	Exp [28].	3.680	5.597	—
	GGA-PBE [28]	—	—	3.56
Tb_2O_3	GGA-PBEsol$^{cal.}$	3.663	5.782	4.11
	HSE06^{cal}	3.665	5.820	5.96
	mbjLDA^{cal}	—	—	6.01
	GGA-PBE [26]	3.714	5.857	—

0), A (0, 0, 1/2), L (1/2, 0, 1/2), and H (1/3, 1/3, 1/2), respectively. Firstly, the electronic band structure and DOS of the Gd_2O_3 and Tb_2O_3 compounds, in which the 4 f states of Gd and Tb atoms are considered as core electrons, were calculated by employing the PBEsol, mbjLDA and HSE06 methods, the results of which are displayed in figure 2. In all three methods, the valence band maximum of the Gd_2O_3 and Tb_2O_3 sesquioxides is located at point Γ, while the conduction band minimum is located at point K. Therefore, the electronic band structures obtained using the GGA-PBEsol, mbjLDA and HSE06 methods demonstrate that the Gd_2O_3 and Tb_2O_3 compounds have an indirect band gap. The band gaps of Gd_2O_3 and Tb_2O_3 compounds were found to be 4.04 eV and 4.11 eV, respectively, using the GGA-PBEsol approach. However, utilising mbjLDA and HSE06 functionals, the band gaps of Gd_2O_3 were determined to be 5.86 eV and 5.61 eV, respectively, while the band gaps of Tb_2O_3 were calculated as 6.01 eV for mbjLDA and 5.69 eV for HSE06. To the best of our knowledge, there are no reported theoretical or experimental band gap values in the literature for A-type hexagonal Gd_2O_3 and Tb_2O_3 compounds, except for [27]. Thanikaivelan *et al* [5] found the optical band gaps of Gd_2O_3 nanoparticles annealed at 500 C, 750 C, and 1000 C to be 5.2 eV, 5.1 eV, and 4.96 eV (in cubic structure) by ultraviolet-visible spectroscopy (UV–Visible DRS), respectively. In other studies, the experimental band gaps of cubic Gd_2O_3 nanoparticles have been reported to be in the energy ranges of 4.41–4.91 eV [29] and 5–5.6 eV [30]. The band gap values we found for hexagonal Gd_2O_3 using the GGA-PBEsol, mbjLDA, and HSE06 methods are close to the values found in [5, 29, 30].

In contrast, the band gap of the Gd_2O_3 and Tb_2O_3 compounds in the GGA + U_{eff} scheme, wherein the 4 f states of the Gd and Tb atoms are considered to be valence electrons, was calculated as a function of U_{eff} and is displayed in figure 3. As seen in figure 3, the band gap of Gd_2O_3 exhibits a rapid increase up to $U_{eff} = 4$ eV. However, after $U_{eff} = 4$ eV, it is seen that the band gap does not change much although U_{eff} increases. Similarly, the band gap of Tb_2O_3 increases up to $U_{eff} = 7$ eV, but the increase slows down after $U_{eff} = 7$ eV. The reason for this can be better understood by carefully analysing the calculated total and partial densities of states for Gd_2O_3 and Tb_2O_3 compounds in figure 4. As seen in figures 4(a) and (b), the effective Hubbard parameter (U_{eff}) has a significant effect on the f-electrons of Gd and Tb atoms. As the value of U_{eff} increases, the 4 f valence states just below the Fermi level shift to lower energies and the 4 f conduction bands just above the Fermi level shift to higher energies. However, the formation of the valence bands just below the Fermi level and the conduction bands just above the Fermi level is contributed not only by the f-orbitals of the Gd and Tb atoms but also by the d-orbitals of the Gd and Tb atoms and the p-orbitals of the O atom. Therefore, although the value of U_{eff} increases, the band gap of both compounds does not increase much.

3.3. Optical properties

The optical properties of a material can be characterised by the complex dielectric function, which defines the relationship between that material and an external electromagnetic field. The complex dielectric function consists of real ($\varepsilon_1(\omega)$) and imaginary ($\varepsilon_2(\omega)$) components, defined as $\varepsilon(\omega) = \varepsilon_1(\omega) + i\varepsilon_2(\omega)$. The real part of the complex dielectric function, designated as $\varepsilon_1(\omega)$, is responsible for the polarization of the material, while the imaginary part, designated as $\varepsilon_2(\omega)$, is related to interband transitions. The imaginary part, known as $\varepsilon_2(\omega)$, is derived from the momentum matrix elements between the occupied and unoccupied states of electrons using the equation given in [31]. Subsequent to the determination of $\varepsilon_2(\omega)$, the value of $\varepsilon_1(\omega)$ is derived from the Kramers–Kronig

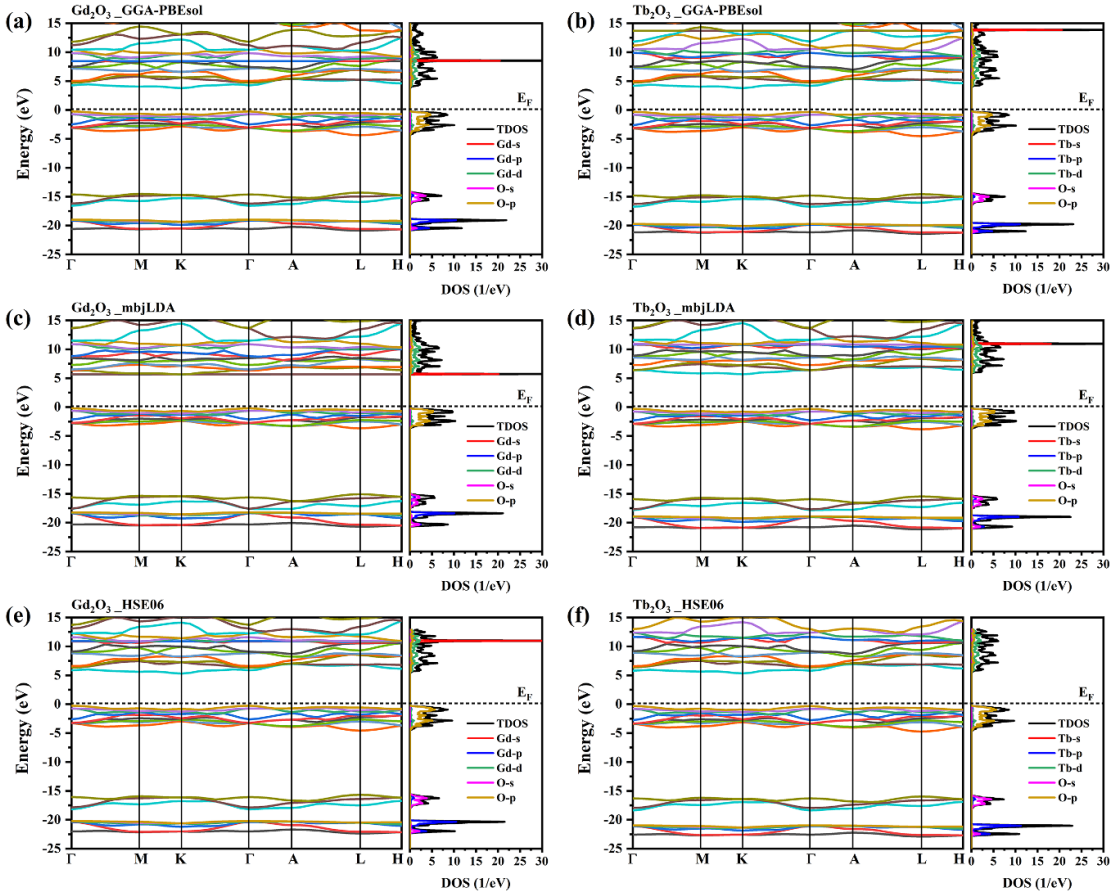


Figure 2. The electronic band structure and DOS of Re_2O_3 sesquioxides calculated using GGA-PBEsol, mbjLDA, and HSE06 methods.

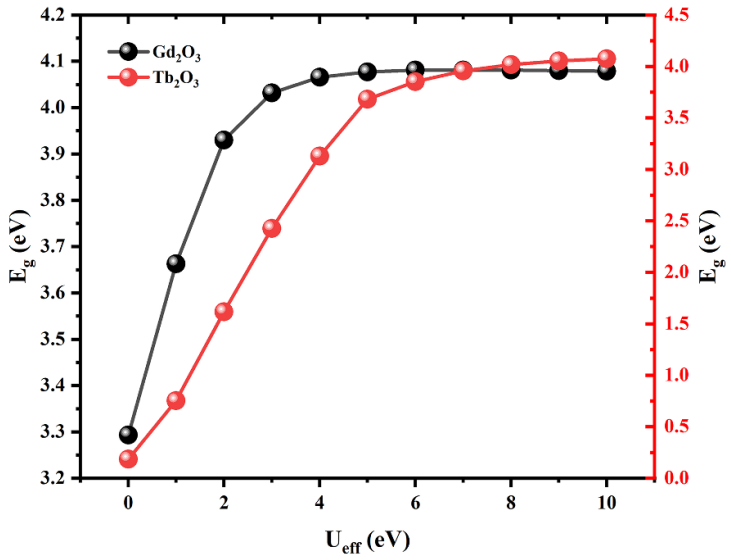


Figure 3. The calculated band gaps of Re_2O_3 sesquioxides as a function of U_{eff}.

relation [31]. Subsequently, other optical properties, including refraction, absorption, energy loss function and reflection, can be derived using $\varepsilon_1(\omega)$ and $\varepsilon_2(\omega)$ [32]. Due to the symmetry of hexagonal Gd_2O_3 and Tb_2O_3 compounds, the dielectric tensor has only three diagonal components (*xx*, *yy*, and *zz*). Since $xx = yy$ for hexagonal structures, the number of independent components is reduced to two. For Gd_2O_3 and Tb_2O_3 compounds, the real and imaginary parts of the dielectric function were calculated in the *x*- and *z*-directions using the GGA-PBEsol, mbjLDA, and HSE06 methods, and the results

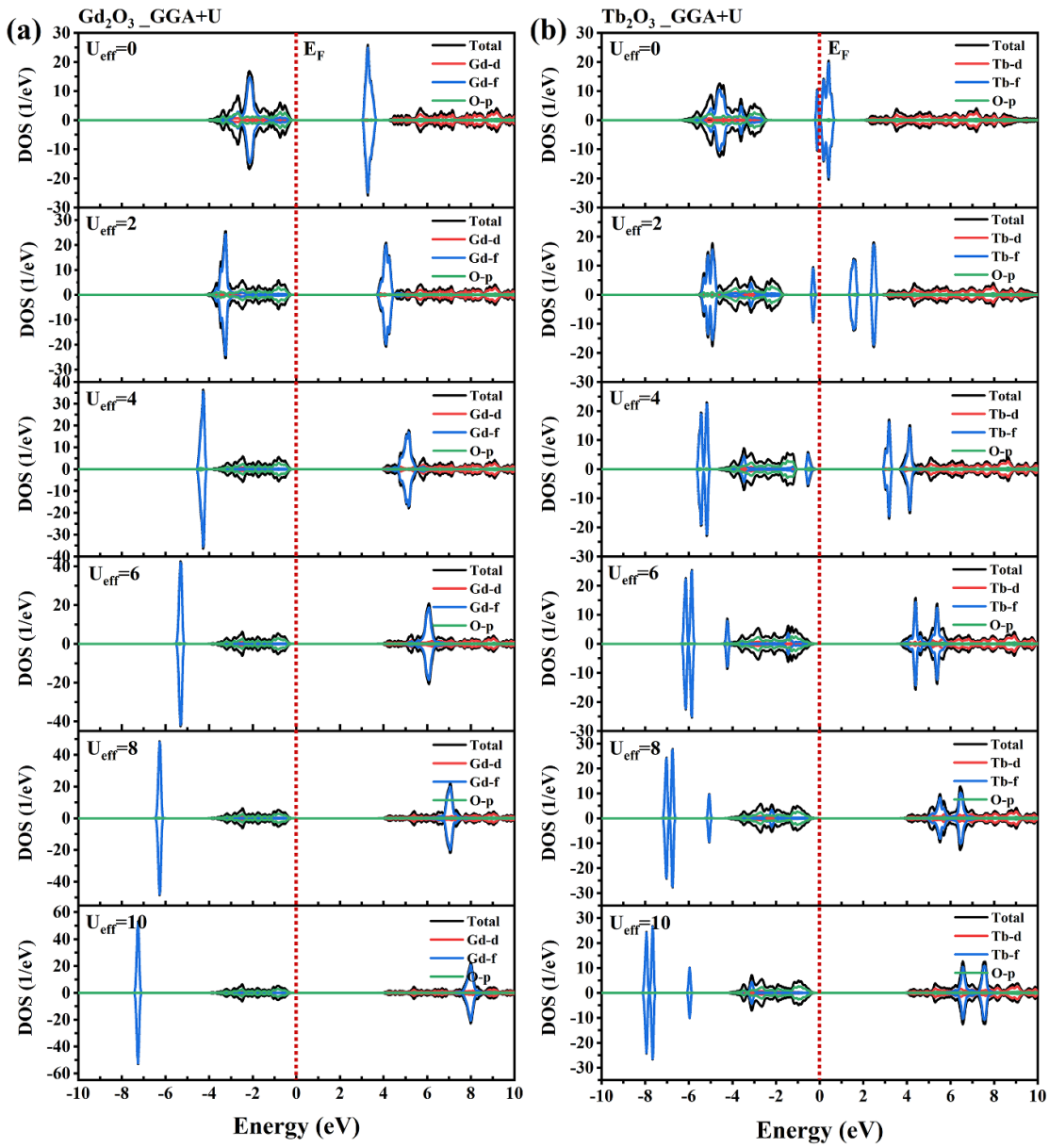


Figure 4. DOS and PDOS of Re_2O_3 sesquioxides calculated for different U_{eff} values.

are shown in figures 5 and 6. In order to gain further insight into the electronic polarizability of materials, it is necessary to know the value of $\varepsilon_1(\omega)$ in the zero-frequency limit, which is known as the static dielectric constant. In calculations performed for the Gd_2O_3 compound, the $\varepsilon_1^{xx}(0)$ values were determined to be 4.92, 3.78, and 3.95 using the GGA-PBEsol, mbjLDA, and HSE06 methods, respectively. The $\varepsilon_1^{zz}(0)$ values for the same compound were determined to be 4.80, 3.66, and 3.81 for these methods, respectively. In a similar manner, the $\varepsilon_1^{xx}(0)$ values of Tb_2O_3 were determined to be 4.86, 3.70, and 3.90, respectively. The $\varepsilon_1^{zz}(0)$ values were found to be 4.73, 3.58, and 3.76, respectively. As indicated in Penn's model [33], when comparing the band gap values obtained using the GGA-PBEsol, mbjLDA, and HSE06 methods for both Gd_2O_3 and Tb_2O_3 with their $\varepsilon_1(0)$ values, it is clearly seen that larger band gap values result in smaller $\varepsilon_1(0)$ values. For the Gd_2O_3 compound, the $\varepsilon_1^{xx}(\omega)$ values obtained using the GGA-PBEsol, mbjLDA, and HSE06 methods take negative values in the 10.0–14.2 eV, 11.0–14.2 eV, and 11.8–15.4 eV ranges, respectively. The $\varepsilon_1^{zz}(\omega)$ values for the same methods show negative values in the 10.0–12.8 eV, 11.1–13.5 eV, and 11.8–14.4 eV ranges, respectively. In contrast, for the Tb_2O_3 compound, the $\varepsilon_1^{xx}(\omega)$ values are negative in the 10.1–14.5 eV (GGA-PBEsol), 11.2–14.5 eV (mbjLDA), and 11.9–16.1 eV (HSE06) ranges, while the $\varepsilon_1^{zz}(\omega)$ values take negative values in the 10.2–12.9 eV (GGA-PBEsol), 11.3–13.8 eV (mbjLDA), and 12.2–14.5 eV (HSE06) ranges. In these specific energy ranges where the real part of the dielectric function becomes negative ($\varepsilon_1(\omega)<0$), the material exhibits a strong plasmonic

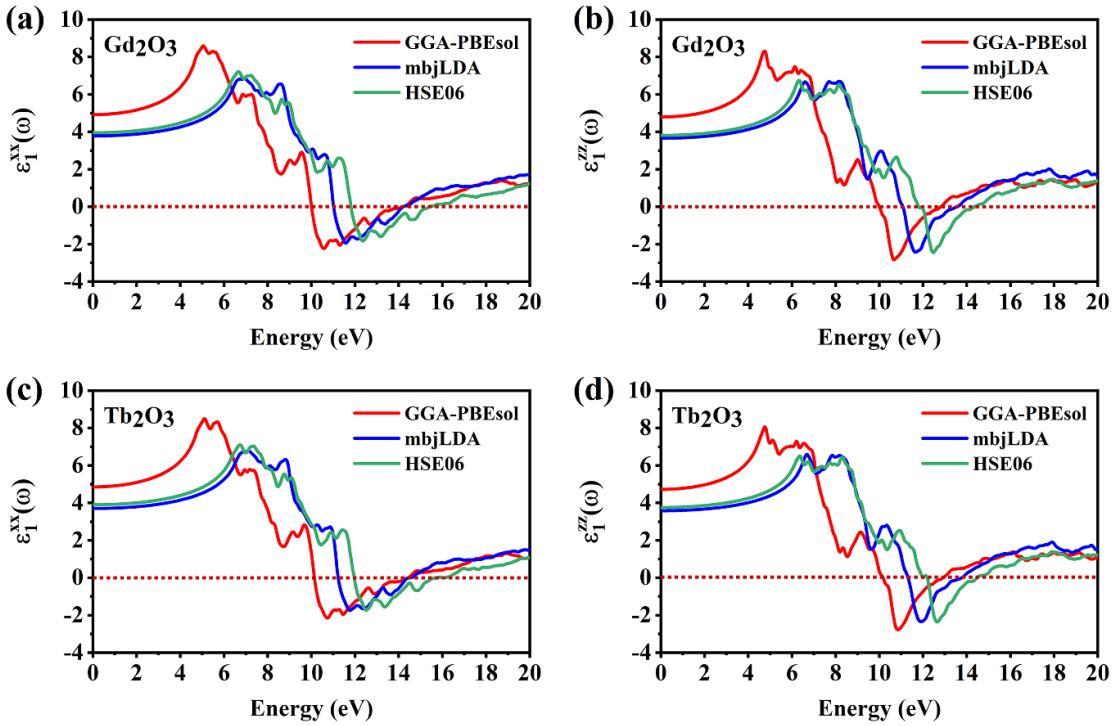


Figure 5. The real part of dielectric function of Re_2O_3 sesquioxides calculated using GGA-PBEsol, mbjLDA, and HSE06 methods.

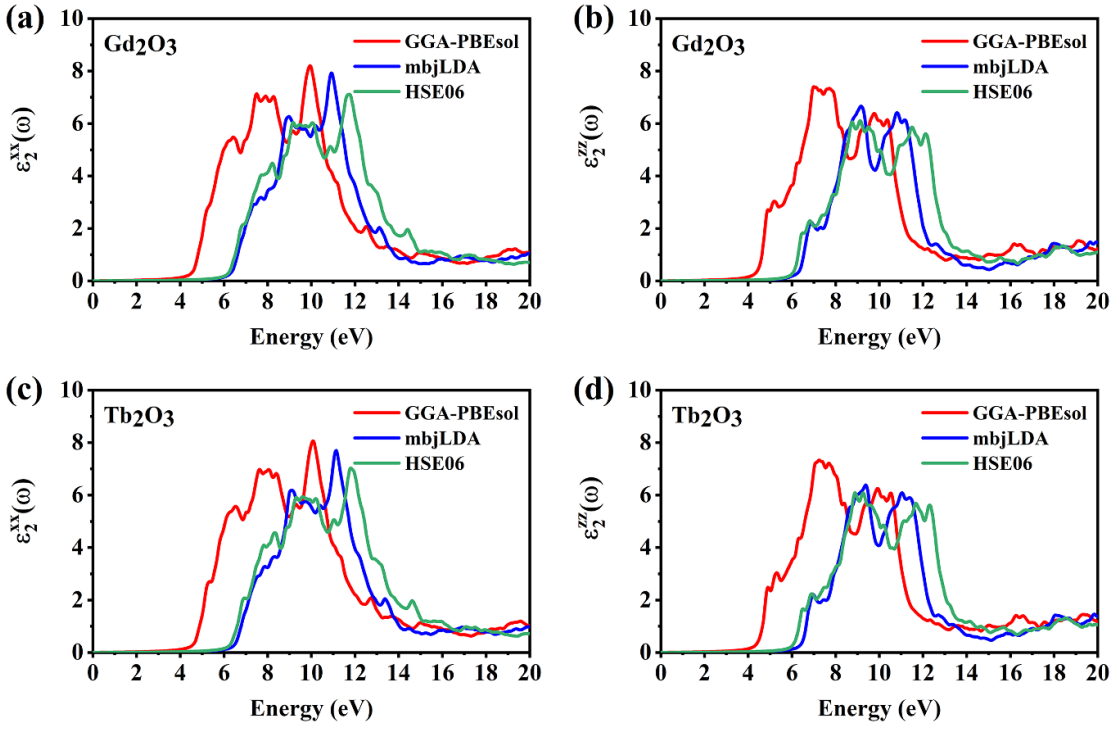


Figure 6. The imaginary part of dielectric function of Re_2O_3 sesquioxides calculated using GGA-PBEsol, mbjLDA, and HSE06 methods.

behaviour and acts as an optical reflector. In this region, the material blocks the propagation of electromagnetic waves and highly reflects the incident electromagnetic waves [34, 35].

Figure 6 shows the imaginary part of the dielectric function related to the material's absorption, which has been calculated for both compounds using the GGA-PBEsol, mbjLDA, and HSE06 methods. The imaginary part $\varepsilon_2(\omega)$ of the dielectric function is directly related to the electronic structure of materials, and the point where the $\varepsilon_2(\omega)$ curve begins to rise indicates the material's optical bandgap, also

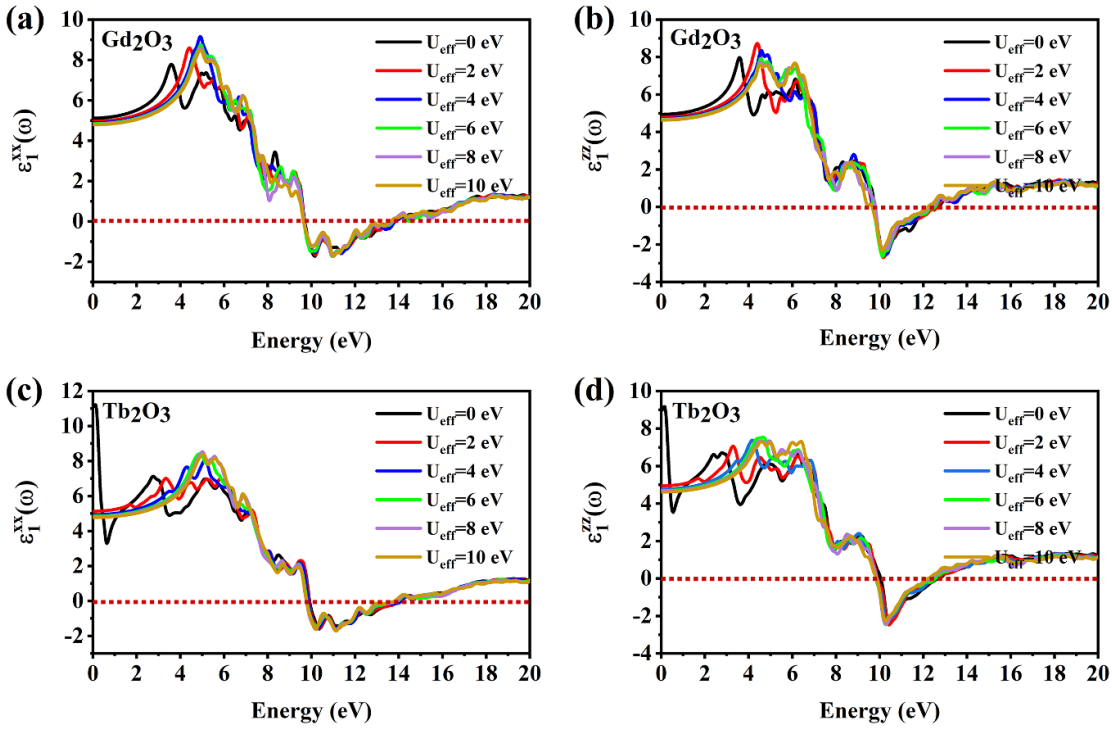


Figure 7. Real part of the dielectric function calculated for different U_{eff} values of Re_2O_3 sesquioxides.

known as the absorption edge or the threshold energy. The threshold energies for Gd_2O_3 are approximately 4.1 eV (GGA-PBEsol), 6.0 eV (mbjLDA), and 5.9 eV (HSE06), respectively. For Tb_2O_3, the threshold energy values are approximately 4.2 eV (GGA-PBEsol), 6.1 eV (mbjLDA), and 6.0 eV (HSE06), respectively, and the obtained values are consistent with the calculated band gap.2 eV (6.5 eV), 8.2 eV (8.3 eV) and 8.9 eV (9.1 eV), respectively, which correspond to the electronic transitions between the O-2p states in the valence band and the Gd(Tb)-5d states in the conduction band. Furthermore, the other peaks observed in the $\varepsilon_2(\omega)$ curve for both compounds are related to electron transitions at different points of the Brilloun zone. On the other hand, as demonstrated in figure 6, the $\varepsilon_2(\omega)$ curves calculated employing the GGA-PBEsol, mbjLDA, and HSE06 methods indicate a high absorption region between 4 and 12 eV for both compounds. The results obtained indicate that Gd_2O_3 and Tb_2O_3 compounds may be suitable for use in UV (ultraviolet) optoelectronic applications.

For both compounds, $\varepsilon_1(\omega)$ values were calculated for different U_{eff} values along the x and z- axes in the GGA + U_{eff} scheme, and the results are shown in figure 7. As seen in figures 7(a) and (b), as U_{eff} increases, the $\varepsilon_1(0)$ values for the x and z-directions decrease slightly. However, despite the increase in U_{eff}, the energy ranges where $\varepsilon_1(\omega)<0$ do not change. On the other hand, as seen in figures 8(c) and (d), when $U_{\text{eff}} = 0$, the $\varepsilon_1(0)$ value is about 13. From figure 3, it is clearly seen that Tb_2O_3 has a band gap of about 0.19 eV when $U_{\text{eff}} = 0$. According to the Penn model $\left(\varepsilon_1(0) = 1 + \left(\hbar\omega_p/E_g\right)^2\right)$ [33], $\varepsilon_1(0)$ is related to the band gap (E_g) and hence the band gap values increase while the $\varepsilon_1(0)$ values decrease as seen in figures 7(c) and (d). The findings demonstrate that both compounds adhere to the Penn model. Furthermore, despite the increase in U_{eff}, it is clearly seen that the energy ranges where $\varepsilon_1(\omega) < 0$ for Tb_2O_3 do not change, just as with the Gd_2O_3 compound.

The $\varepsilon_2(\omega)$ curves calculated using the GGA + U_{eff} method for both compounds are shown in figure 8. As demonstrated in figure 8, the threshold energies exhibit a shift towards higher energies, depending on the U_{eff} values. This shift is observed up to $U_{\text{eff}} = 4$ eV for Gd_2O_3 and up to $U_{\text{eff}} = 7$ eV for Tb_2O_3. However, despite the increase in U_{eff}, the threshold energy values remain constant. The reason for this is that the imaginary part of the dielectric function of the materials studied is directly related to the DOS and will be better understood when figure 4 is examined. When the U_{eff} correction is applied to the 4 f electrons of Gd and Tb atoms, the 4 f states in the valence and conduction bands expand, as is evident in the DOS plot in figure 4. Concurrently, the O-2p and Gd(Tb)-5d states also contribute to the formation of the bands immediately below and above the Fermi level. Consequently, despite the expansion of the 4 f states, the band gap remains constant after $U_{\text{eff}} = 4$ eV for Gd_2O_3 and $U_{\text{eff}} = 7$ eV for Tb_2O_3, indicating that the threshold energy values remain unchanged.

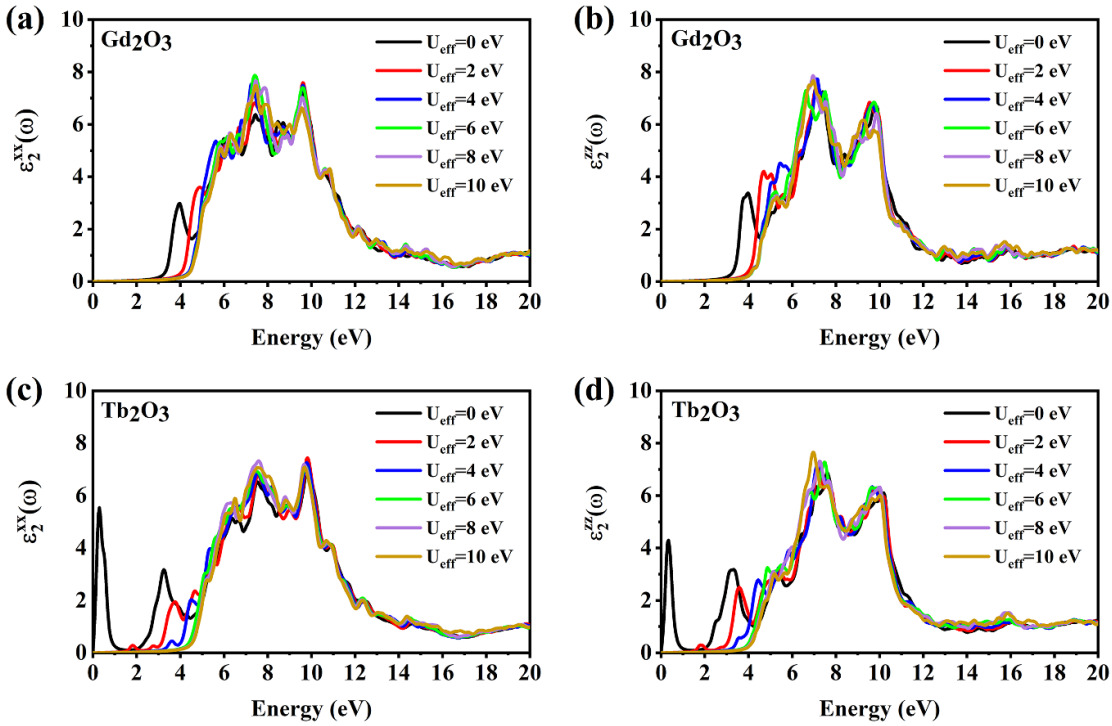


Figure 8. Imaginary part of the dielectric function calculated for different U_{eff} schemes of Re_2O_3 sesquioxides.

Table 2. The calculated elastic constants C_{ij} (GPa) of Re_2O_3 sesquioxides.

Material	References	C_{11}	C_{12}	C_{13}	C_{14}	C_{33}	C_{44}
Gd_2O_3	GGA-PBEsol$^{cal.}$	261.9	151.9	102.4	44.9	177.3	86.0
	HSE06$^{cal.}$	267.2	154.7	102.1	49.5	182.5	86.7
	GGA-PBE [27]	263.0	155.5	110.6	—	174.8	53.7
Tb_2O_3	GGA-PBEsol$^{cal.}$	269.2	155.8	105.1	47.1	180.2	90.0
	HSE06$^{cal.}$	271.7	151.2	101.7	51.9	187.4	90.4

3.4. Elastic Properties

In order to determine the mechanical properties of a material, elastic constants need to be known. Elastic constants help us to understand the behaviour of materials such as mechanical stability, hardness, softness, brittleness, ductility, anisotropy and also to obtain polycrystalline elastic moduli such as bulk modulus, shear modulus, Young's modulus [36]. Gd_2O_3 and Tb_2O_3 compounds belong to the hexagonal crystal system and have eight components: C_{11}, C_{12}, C_{13}, C_{14}, C_{33}, C_{44}, C_{65} and C_{66}. Since $C_{66} = 1/2\,(C_{11} - C_{12})$ and $C_{14} = C_{65}$, the number of independent components is reduced to six. The elastic constants calculated by GGA-PBEsol and HSE06 for Gd_2O_3 and Tb_2O_3 compounds are given in table 2. The mechanical stability condition for hexagonal crystals must satisfy the Born stability criteria [37] given by equation (3.1) below

$$\begin{gathered}(C_{11} - C_{12}) > 0, (C_{11} + C_{12}) > 0,\ C_{33} > 0,\ C_{44} > 0 \\ (C_{11} + C_{12})\,C_{33} - 2C_{13}^2 > 0,\ (C_{11} - C_{12})\,C_{44} - 2C_{14}^2 > 0\end{gathered} \tag{3.1}$$

As illustrated in table 2, both crystals satisfy the Born stability criteria, as expressed in equation (4.1). Consequently, it can be concluded that both Gd_2O_3 and Tb_2O_3 crystals exhibit mechanical stability.

As illustrated in table 2, the values of the elastic constants calculated by GGA-PBEsol and HSE06 for both compounds are found to be highly similar. In addition, it is seen that the elastic constants calculated by GGA-PBEsol and HSE06 for Gd_2O_3 are in close agreement with the other values of elastic constants, with the exception of the C_{13} and C_{44} elastic constants when compared with the results reported in [27]. The elastic constants C_{11} and C_{33} are defined as the resistance of the material to linear compression along the [100] (x-axis) and [001] (z-axis) directions, respectively [38, 39]. As illustrated in table 2, the C_{11} parameter is larger than the C_{33} parameter for both the Gd_2O_3 and Tb_2O_3 compounds. This

Table 3. The calculated bulk modulus B (GPa), shear modulus G (GPa), Young's modulus E (GPa), Vickers hardness (GPa), B/G ratios and Poisson's ratio (ν) of Re_2O_3 sesquioxides.

Material	References	B_V	B_R	B	G_V	G_R	G	E	H_C	H_T
Gd_2O_3	GGA-PBEsol[cal.]	157.2	146.1	151.6	68.4	41.0	54.7	145.8	3.30	4.91
	HSE06[cal.]	159.4	148.3	153.9	69.8	37.1	53.4	142.6	2.94	4.62
	GGA-PBE [27]	150.8	149.5	150.1	69.6	64.7	67.1	175.3	—	—
	Exp. [28]	—	—	160	—	—	—	—	—	—
	Exp. [46]	—	—	174	—	—	—	—	—	—
Tb_2O_3	GGA-PBEsol[cal.]	161.2	149.3	155.2	70.8	41.8	56.3	150.1	3.46	5.04
	HSE06[cal.]	160.0	149.8	154.9	73.3	39.7	56.5	150.1	3.51	5.09

indicates that the compressibility of both crystals along the [100] direction is stronger than the compressibility along the [001] direction. The elastic constant C_{44} represents the resistance to shear deformation of the crystal with respect to the tangential stress applied to the (100) plane in the [010] direction [40]. As can be seen from table 2, C_{44} values are smaller than C_{11} and C_{33} values for Gd_2O_3 and Tb_2O_3 compounds. From these results, it appears that Re_2O_3 compounds can be more easily deformed by a shear than by a unidirectional stress along any of the x-, y- or z-base axes.

In addition to the hardness values calculated according to the Chen (H_C) [41] and Tian (H_T) [42] models for Gd_2O_3 and Tb_2O_3 compounds, the bulk modulus (B), shear modulus (G) and Young's modulus (E) were also calculated and are given in table 3. The mechanical properties of the studied Re_2O_3 compounds in polycrystalline form can be determined from the single-crystal elastic constants using two fundamental methods known as the Voigt [43] and Reuss [44] methods. The Voigt (V) approach assumes uniform strain in the structure and gives the upper limit for the parameters expressed in terms of the elastic coefficients C_{ij}. In the Reuss (R) approach, a uniform stress distribution in the structure is assumed and gives the lower limit for the parameters expressed through the elastic compliance tensor S_{ij}. The terms B_V (G_V) and B_R (G_R) presented in table 3 represent the Voigt and Reuss bounds for the bulk (shear) modulus, respectively. According to the Voigt–Reuss–Hill approach, the polycrystalline bulk modulus (B) and shear modulus (G) are determined by taking the arithmetic mean of these two limits ($B = (B_V + B_R)/2$ and $G = (G_V + G_R)/2$) [45]. As can be seen in table 3, the B, G and E values of Tb_2O_3 are higher than those of Gd_2O_3. Consequently, the Tb_2O_3 crystal is harder and exhibits greater resistance to compression and plastic deformation. On the other hand, the B values we found for the Gd_2O_3 compound are very close to those found by Islam *et al* [27]. However, the G and E values we found for both compounds are lower than the results found by Islam *et al* [27].

On the other hand, the effects of the U_{eff} parameter on Gd_2O_3 and Tb_2O_3 compounds were investigated. The elastic constants and elastic moduli calculated for different U_{eff} parameters are given in figure 9. As can be seen from figure 9, the U_{eff} parameter has no significant effect on the elastic properties of both compounds.

The hardness of a material is related to its elasticity and plasticity properties. In this study, the hardness of Gd_2O_3 and Tb_2O_3 compounds was estimated using the Chen *et al* [41] and Tian *et al* [42] models, and the hardness values of these compounds are given in table 3. As can be seen from table 3, there is a relationship between both H_C and H_T hardness values of the Gd_2O_3 and Tb_2O_3 compounds as $Tb_2O_3 > Gd_2O_3$. In other words, Tb_2O_3 is seen to be a harder material than Gd_2O_3. According to the literature, materials with a hardness value below 10 GPa are categorised as soft materials [47], while those with a hardness value above 40 GPa are classified as superhard materials [48]. As demonstrated in table 3, given that the hardness values of the Gd_2O_3 and Tb_2O_3 compounds are less than 10 GPa according to both models, these materials can be classified as soft materials. The B/C_{44} ratio defines the machinability index, which is an important performance indicator for solids. The machinability of a solid is related to its hardness, and a softer solid can be shaped more easily [36]. The machinability indices obtained with GGA-PBEsol (HSE06) for the Gd_2O_3 and Tb_2O_3 compounds were found to be 1.76 (1.78) and 1.72 (1.71), respectively. It can thus be concluded that the Gd_2O_3 compound is more amenable to shaping when compared to the Tb_2O_3 compound.

In accordance with the criteria established by Pugh [49], the nature of the materials, namely whether ductile ($B/G > 1.75$) or brittle ($B/G < 1.75$), can be ascertained. The calculated B/G ratios for the Gd_2O_3 and Tb_2O_3 compounds are presented in table 4. As demonstrated in table 4, the B/G ratios calculated with GGA-PBEsol and HSE06 for both compounds exceed 1.75. Consequently, both compounds demonstrate ductile behaviour. Poisson's ratio (ν) generally represents the stability of a solid against shear deformation. The value of Poisson's ratio normally varies between -1 and 0.5 for a stable and linear

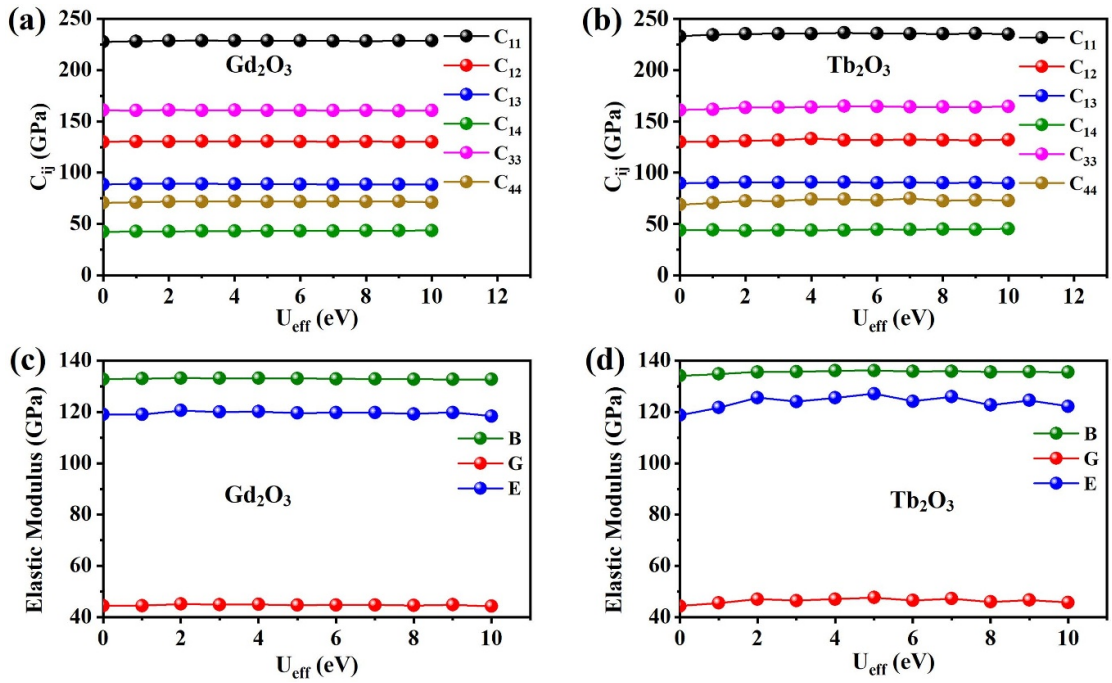


Figure 9. The calculated elastic constants and elastic moduli of Re_2O_3 sesquioxides as a function of U_{eff}.

Table 4. The calculated Pugh's ratio (B/G), Poisson's ratio (ν) and anisotropy factors (A) of Re_2O_3 sesquioxides.

Material	References	B/G	ν	A_1	A_2	A_3	A^U
Gd_2O_3	GGA-PBEsol$^{cal.}$	2.77	0.339	1.468	1.468	1.00	3.409
	HSE06$^{cal.}$	2.88	0.344	1.413	1.413	1.00	4.487
	GGA-PBE [27]	2.23	0.30	—	—	—	0.045
Tb_2O_3	GGA-PBEsol$^{cal.}$	2.76	0.338	1.505	1.505	1.00	3.543
	HSE06$^{cal.}$	2.74	0.337	1.414	1.414	1.00	4.290

elastic solid. A large value of Poisson's ratio indicates that the solid has good plasticity [50]. As seen in table 4, the Poisson's ratio values of Gd_2O_3 and Tb_2O_3 compounds calculated with GGA-PBEsol(HSE06) were found to be 0.339 (0.344) and 0.338(0.337), respectively, and these values are in the range of −1–0.5. These results indicate that Gd_2O_3 and Tb_2O_3 compounds are stable and linear elastic solids. Usually, the ductility and brittle nature of solids are evaluated by Poisson's ratio ν and B/G. A solid is ductile if it satisfies the conditions $\nu > 0.26$ and $B/G > 1.75$, otherwise it is brittle. As seen in table 4, since $\nu > 0.26$ and $B/G > 1.75$ for Gd_2O_3 and Tb_2O_3 compounds, these crystals are seen to be ductile materials. On the other hand, as seen in table 4, the B/G ratio and ν values obtained by us with GGA-PBEsol(HSE06) for both compounds are higher than the results found by Islam *et al* [27]. The elastic anisotropy is one of the important physical properties of solids, which has an important place in crystal physics and engineering science, including microcrack formation, precipitation, phase transformations and dislocation dynamics. Among them, microcrack formation is of special importance as it affects the mechanical properties of the material. Therefore, it is very important to calculate the elastic anisotropy to understand the mechanism of microcrack formation in order to increase the stiffness of the material [51]. The shear anisotropic factors (A_1, A_2 and A_3), and the universal elastic anisotropy index (A^U) values calculated with GGA-PBEsol and HSE06 for Gd_2O_3 and Tb_2O_3 compounds are presented in table 4. These elastic anisotropy index values indicate that the solid is elastically isotropic when A_1=A_2=A_3 = 1 and A^U = 0. Otherwise, deviation from these values indicates that the solid is elastically anisotropic [50]. As illustrated in table 4, the value of A_3 for Gd_2O_3 and Tb_2O_3 compounds is equivalent to 1, while the values of A_1 and A_2 are distinct from 1. This indicates that for both crystals, the (001) plane manifests isotropic behaviour, whereas the (100) and (010) planes exhibit anisotropic behaviour. On the other hand, as seen in table 4, the universal elastic anisotropy index values calculated for both compounds are different from zero. In summary, it can be concluded that Gd_2O_3 and Tb_2O_3 compounds are anisotropic in nature. The universal elastic anisotropy index (A^U) value was found to

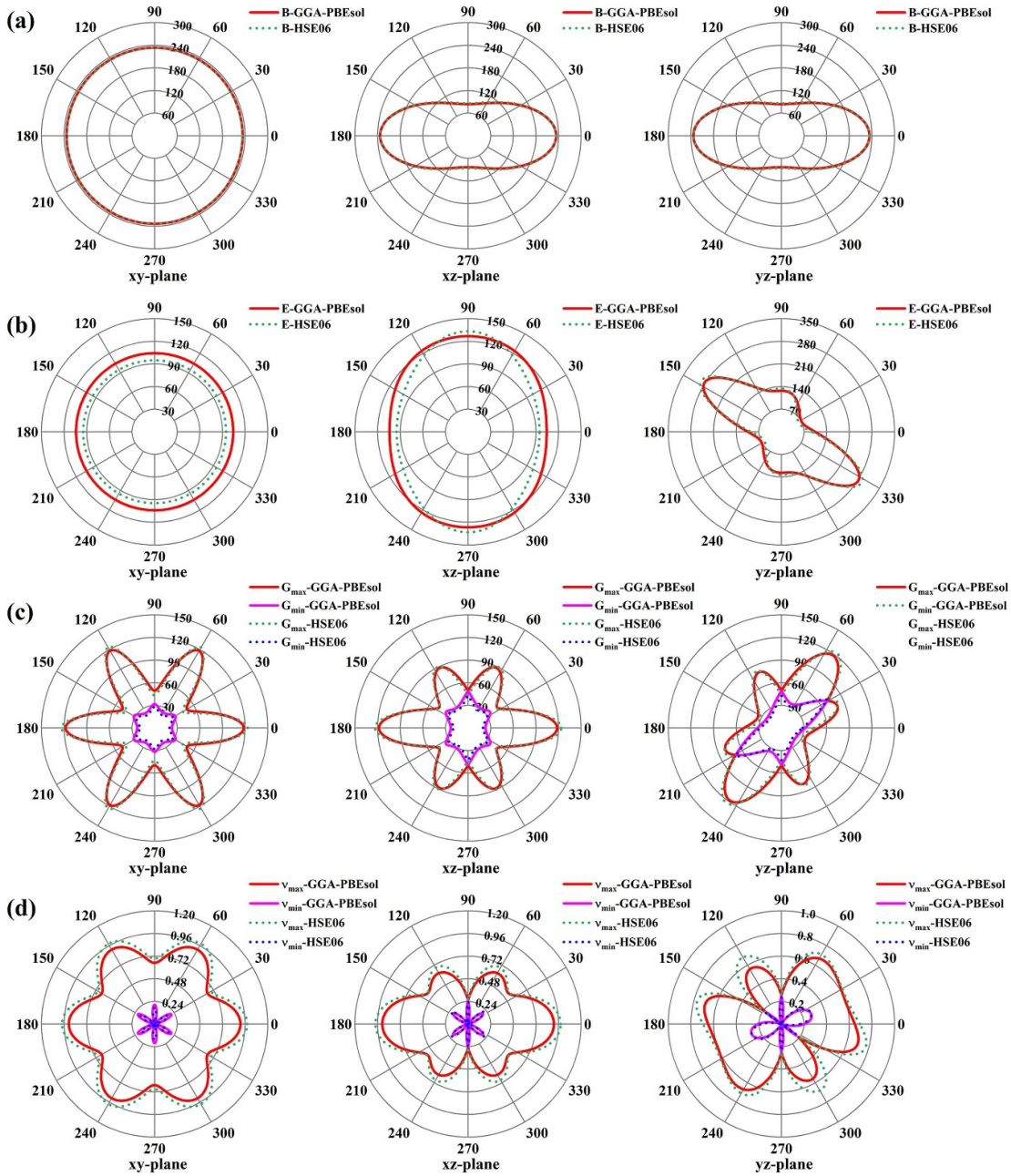


Figure 10. 2D representation of bulk modulu (a), Young modulu (b), shear modulu (c) and Poisson ratio (d) for Gd_2O_3.

be 0.39 by Islam *et al* [27]. This value is greater than the value we found. To better understand the elastic anisotropic nature of Gd_2O_3 and Tb_2O_3 compounds, two-dimensional (2D) orientation-dependent plots of the Bulk modulus, Shear modulus, Young's modulus, and Poisson's ratio were plotted in the *xy, xz,* and *yz* planes using VELAS code [52], with the results provided in figures 10 and 11. The circular shapes indicate the isotropic nature of the material, while deviations from circular shapes express the anisotropic nature of the material. As demonstrated in figures 10(a) and (b) and 11(a) and (b), the Bulk modulus and Young's modulus of both compounds exhibit a circular shape in the *xy* plane, but show significant deviations from the circular form in the *xz* and *yz* planes. This indicates that both compounds have an isotropic structure in the *xy* plane, but exhibit highly anisotropic behaviour in the *xz* and *yz* planes. On the other hand, as seen in figures 10(c) and (d) and 11(c) and (d), both the Shear modulus and the Poisson's ratio exhibit significant deviations from the circular form in the *xy, xz*, and *yz* planes. This suggests that the Shear modulus and Poisson's ratio of the Gd_2O_3 and Tb_2O_3 compounds have high anisotropy in all three planes.

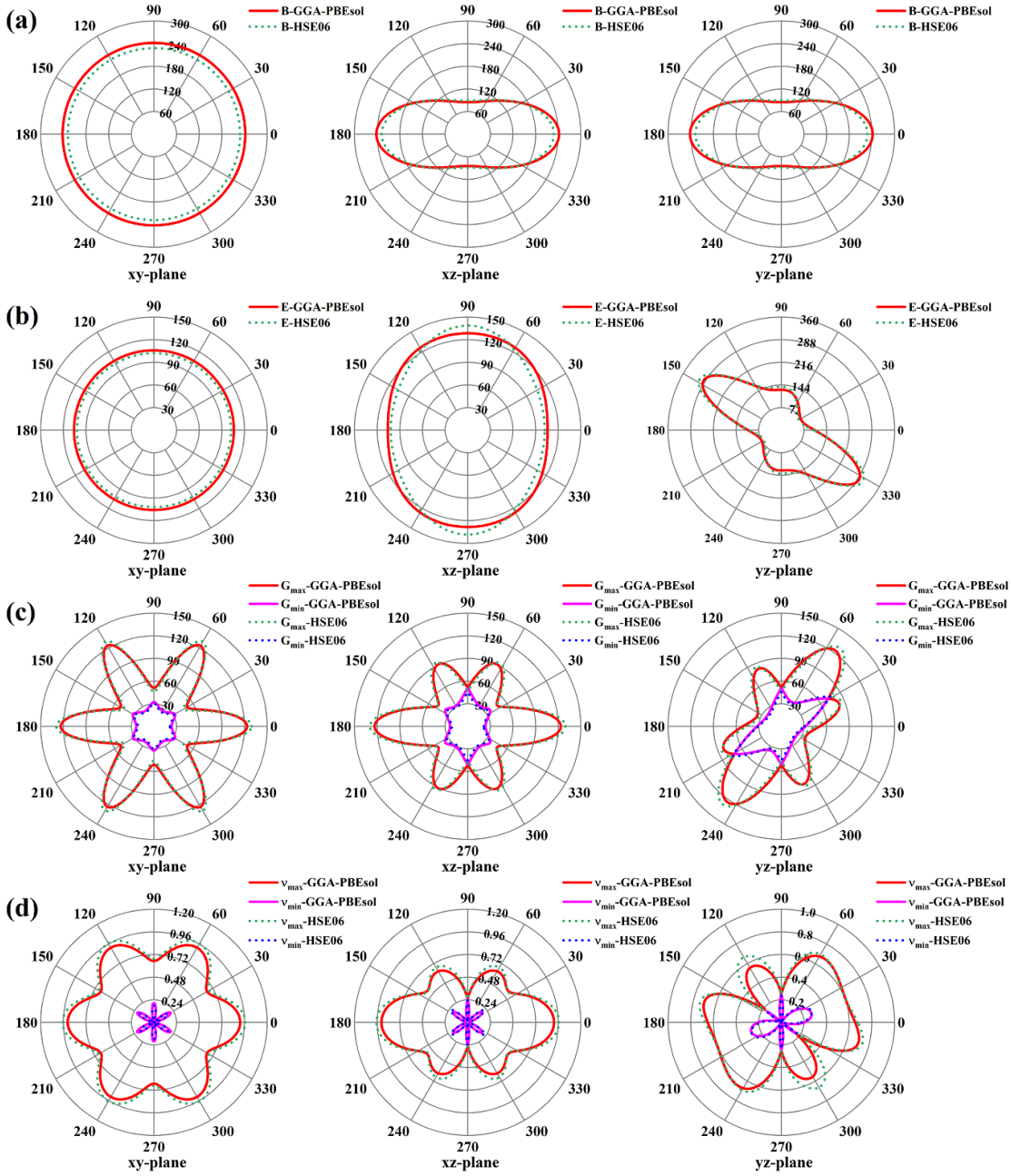


Figure 11. 2D representation of bulk modulu (a), Young modulu (b), shear modulu (c) and Poisson ratio (d) for Tb_2O_3.

4. Conclusions

In conclusion, the structural, magnetic, electronic, optical and mechanical properties of A-type Re_2O_3 (Re = Gd, Tb) rare earth sesquioxides were investigated by first-principles calculations using different approaches including GGA-PBEsol, mbjLDA, HSE06 and GGA + U_{eff}. The structural optimization results of the investigated compounds are in good agreement with the results in the literature. According to our calculations, Gd_2O_3 and Tb_2O_3 compounds are magnetic insulator materials with indirect band gap. The indirect electronic band gaps calculated by GGA-PBEsol, mbjLDA, and HSE06 methods are 4.04 eV, 5.86 eV, and 5.61 eV for Gd_2O_3, while they are 4.11 eV, 6.01 eV, and 5.96 eV for Tb_2O_3, respectively. The calculated magnetic moments of Gd and Tb atoms are 6.926 μB and 5.916 μB, respectively. Optical properties were investigated in the 0–20 eV energy range and from the results obtained, it was evaluated that both compounds could be suitable for UV optoelectronic applications. From the calculation of elastic constants, it is understood that these materials meet the Born mechanical stability criteria and are mechanically stable. Pugh and Poisson's ratios show that both Gd_2O_3 and Tb_2O_3 are ductile in structure, and the hardness values calculated from the Chen and Tian model show that

both compounds are soft materials. From shear anisotropic factors and 2D plots, it is understood that the bulk modulus and Young modulus of both the compounds exhibit isotropic behaviour in the *xy* plane, but anisotropic behaviour in the *xz* and *yz* planes. On the other hand, due to the strong correlation between f electrons of Gd and Tb atoms, the effect of the U_{eff} parameter on the electronic, optical, magnetic and elastic properties of both compounds was investigated. The results obtained indicate that the U_{eff} parameter affects the electronic, magnetic, and optical properties, but has no significant effect on the structural and mechanical properties.

Data availability statement

All data that support the findings of this study are included within the article (and any supplementary files).

Conflict of interest

The authors declare that they have no known competing financial interests or personal relationships that could have appeared to influence the work reported in this paper.

Author contribution

Sedat Durman
Data curation (equal), Investigation (equal), Resources (equal), Validation (equal), Visualization (equal)

References

[1] Pedersen H and Ojamäe L 2006 Towards biocompatibility of REO nanocrystals -: water and organic molecules chemisorbed on GdO and YO nanocrystals studied by quantum-chemical computations *Nano Lett.* **6** 2004
[2] Lonappan D, Chandra Shekar N V, Sahu P C, Kumarasamy B V, Bandyopadhyay A K and Rajagopalan M 2008 Cubic to hexagonal structural transformation in Gd_2O_3 at high pressure *Philos. Mag. Lett.* **88** 473
[3] Hiti A, Nekkach F, Boutahar A, Moubah R, Lemziouka H and Hlil E K 2023 Effects of Mn doping on the structural, linear and nonlinear optical properties of Gd_2O_3 nanoparticles *Opt. Mater.* **143** 114161
[4] Garg A B, Muñoz A, Anzellini S, Sánchez-martín J, Turnbull R, Díaz-anichtchenko D, Popescu C and Errandonea D 2024 Role of GdO addition in the structural stability of cubic Gd_2O_3 at high pressures: determination of the equation of states of GdO and Gd_2O_3 *Materialia* **34** 102064
[5] Thanikaivelan E, Raj S G, Saravanan L and Murugakoothan P 2025 Structure, thermal stability, particle size, photoluminescence and magnetic measurement of gadolinium oxide nanoparticles: a simple method *J. Alloy Compd.* **1046** 184639
[6] Jegadeesan P, Sen S, Srivastava S K, Padmaprabu C, Dasgupta A and Amirthapandian S 2024 Investigations on ion irradiation induced microstructural changes in Gd_2O_3 nanorods *Radiat. Phys. Chem.* **222** 111858
[7] Islam M and Sheikh M A R 2024 Predicting the stability and exploring the fundamental physical properties of tetragonal Gd_2O_3: a comprehensive first-principles investigation *Nucl. Mater. Energy* **41** 101734
[8] Grosse F, Watahiki T and Braun W 2010 Rare earth oxide alloys and stacked layers: an *ab initio* study *Thin Solid Films* **518** 4747
[9] Horoz S, Simsek S, Palaz S and Mamedov A M 2015 Electronic and optical properties of rare earth oxides: *ab initio* calculation *World J. Condens. Matter Phys.* **05** 78–85
[10] Tamrakar R K, Bisen D P and Brahme N 2016 Structural characterization of Er^{3+},Yb^{3+}-doped Gd_2O_3 phosphor, synthesized using the solid-state reaction method, and its luminescence behaviour *Luminescence* **31** 8–15
[11] Tamrakar R K, Bisen D P and Bramhe N 2015 Influence of Er^{3+} concentration on the photoluminescence characteristics and excitation mechanism of Gd_2O_3:Er^{3+} phosphor synthesized via a solid-state reaction method *Luminescence* **30** 668
[12] Han X, *et al* 2024 Formation and magneto-optical properties of Tb_2O_3-doped gallium borate glass *J. Non-Cryst. Solids* **639** 123108
[13] Zhang J, Chen H, Wang J, Wang D, Han D, Zhang J and Wang S 2019 Phase transformation process of Tb_2O_3 at elevated temperature *Scr. Mater.* **171** 108
[14] Zhou D, Qi H, Wang T, Li W, Jing W, Liu L, Shi Y and Xu J 2023 Effect of La_2O_3 on the microstructure and optical performance of $(Tb_{0.8}Y_{0.2-x}La_x)_2O_3$ ceramics *Ceram. Int.* **49** 4695
[15] Kresse G and Furthmuller J 1996 Efficient iterative schemes for *ab initio* total-energy calculations using a plane-wave basis set *Phys. Rev. B* **54** 11169
[16] Kresse G and Furthmuller J 1996 Efficiency of *ab-initio* total energy calculations for metals and semiconductors using a plane-wave basis set *Comput. Mater. Sci.* **6** 15–50
[17] Perdew J P, Ruzsinszky A, Csonka G I, Vydrov O A, Scuseria G E, Constantin L A, Zhou X and Burke K 2008 Restoring the density-gradient expansion for exchange in solids and surfaces *Phys. Rev. Lett.* **100** 136406
[18] Tran F and Blaha P 2009 Accurate band gaps of semiconductors and insulators with a semilocal exchange-correlation potential *Phys. Rev. Lett.* **102** 226401
[19] Heyd J, Scuseria G E and Ernzerhof M 2003 Hybrid functionals based on a screened Coulomb potential *J. Chem. Phys.* **118** 8207
[20] Kresse G and Joubert D 1999 From ultrasoft pseudopotentials to the projector augmented-wave method *Phys. Rev. B* **59** 1758–75
[21] Le Page Y and Saxe P 2001 Symmetry-general least-squares extraction of elastic coefficients from *ab initio* total energy calculations *Phys. Rev. B* **63** 174103

[22] Le Page Y and Saxe P 2002 Symmetry-general least-squares extraction of elastic data for strained materials from *ab initio* calculations of stress *Phys. Rev. B* **65** 104104
[23] Suter U and Eichinger B 2002 Estimating elastic constants by averaging over simulated structures *Polymer* **43** 575
[24] Liechtenstein A, Anisimov V I and Zaanen J 1995 Density-functional theory and strong interactions: orbital ordering in Mott-Hubbard insulators *Phys. Rev. B* **52** R5467
[25] Momma K and Izumi F 2011 VESTA 3for three-dimensional visualization of crystal,volumetric and morphology data *J. Appl. Crystallogr.* **44** 1272
[26] Wu B, Zinkevich M, Aldinger F, Wen D and Chen L 2007 *s* study on structure and phase transition of A- and B-type rare-earth sesquioxides Ln_2O_3 (Ln=La–Lu, Y, and Sc) based on density function theory *J. Solid State Chem.* **180** 3280
[27] Islam M, Rajak P and Bhattacharyya S 2019 *Ab initio* calculation insights into the structural, elastic and mechanical properties of high-*k* dielectric gadolinium oxide (Gd_2O_3) *Appl. Phys. A* **125** 746
[28] Zhang F X, Lang M, Wang J W, Becker U and Ewing R C 2008 Structural phase transitions of cubic Gd_2O_3 at high pressures *Phys. Rev. B* **78** 064114
[29] Bhoi H, Tiwari S, Manisha H, Pascual L and Kumar S 2024 Structural, optical, luminescent and magnetic properties of Gd_2O_3 nanoparticles: a comparative study on the effect of different green fuels in the sol–gel synthesis tactics *Inorg. Chem. Commun.* **170** 113487
[30] Dhananjaya N, Nagabhushana H, Nagabhushana B M, Rudraswamy B, Sharma S C, Sunitha D V, Shivakumara C and Chakradhar R P S 2012 Effect of different fuels on structural, thermo and photoluminescent properties of Gd_2O_3 nanoparticles *Spectrochim. Acta B* **96** 532
[31] Maskar E, Lamrani A F, Belaiche M, Es-smairi A, Khuili M, Al-qaisi S, Vu T V and Rai D P 2021 Electronic, magnetic, optical and transport properties of wurtzite-GaN doped with rare earth (RE = Pm, Sm, and Eu): first principles approach *Surf. Interfaces* **24** 101051
[32] Shen Y Q and Zhou Z X 2008 Structural, electronic, and optical properties of ferroelectric $KTa_{1/2}Nb_{1/2}O_3$ solid solutions *J. Appl. Phys.* **103** 074113
[33] Reshak A H 2015 Specific features of electronic structures and optical susceptibilities of molybdenum oxide *RSC Adv.* **5** 22044
[34] Siddiqua A, Jui J A, Ahmed S, Bhuyan M D I and Obaidullah 2026 First-principles calculation of rhombohedral perovskite MgAgF3: a DFT study of optical, electronic, elastic, thermodynamic and mechanical properties *Mater. Adv.* **7** 2675
[35] Song D *et al* 2026 Enhanced light–matter interaction in plasmonic nanocavities: principle, challenge, and perspective *Photon. Insights* **5** R01
[36] Ali M A, Hossain M M, Islam A K M A and Naqib S H 2021 Ternary boride Hf_3PB_4: insights into the physical properties of the hardest possible boride MAX phase *J. Alloy Compd.* **857** 158264
[37] Wang W, Wang R, Zhang W, Xing L L, Xu Y L and Wu X H 2013 A computer study and photoelectric property analysis of potassium-doped lithium niobate single crystals *Phys. Chem. Chem. Phys.* **15** 14347
[38] Koc H, Mamedov A M, Deligoz E and Ozisik H 2012 First principles prediction of the elastic, electronic, and optical properties of Sb_2S_3 and Sb_2Se_3 compounds *Solid State Sci.* **14** 1211
[39] Kaya F, Koc H, Mamedov A M and Ozbay E 2024 The structural, elastic, electronic, and optical properties of the rhombohedral La_2NiMnO_6 double perovskite compound at different temperatures *Comput. Condens. Matter* **41** e00984
[40] Naher M I, Afzal M A and Naqib S H 2021 A comprehensive DFT based insights into the physical properties of tetragonal superconducting Mo_5PB_2 *Results Phys.* **28** 104612
[41] Chen X-Q, Niu H, Li D and Li Y 2011 Modeling hardness of polycrystalline materials and bulk metallic glasses *Intermetallics* **19** 1275
[42] Tian Y, Xu B and Zhao Z 2012 Microscopic theory of hardness and design of novel superhard crystals *Int. J. Refract. Met. Hard Mater.* **33** 93–106
[43] Voigt W 1910 Lehrbuch der Kristallphysik (Teubner Verlag)
[44] Reuss A 1929 Calculation of the flow limits of mixed crystals on the basis of the plasticity of monocrystals *Z. Angew. Math. Mech.* **9** 49
[45] Hill R 1952 The elastic behaviour of a crystalline aggregate *Proc. Phys. Soc. A* **65** 349
[46] Bai L G, Liu J, Li X D, Jiang S, Xiao W, Li Y, Tang L, Zhang Y and Zhang D 2009 Pressure-induced phase transformations in cubic Gd_2O_3 *J. Appl. Phys.* **106** 073507
[47] Liu W N, Niu Y T and Li W Q 2020 Theoretical prediction of the physical characteristic of Na_3MO_4 (M=Np and Pu): the first-principles calculations *Ceram. Int.* **46** 25359
[48] Haines J, Léger J M and Bocquillon G 2001 Synthesis and design of superhard materials *Annu. Rev. Mater. Res.* **31** 1–23
[49] Pugh S 1954 XCII. Relations between the elastic moduli and the plastic properties of polycrystalline pure metals the London, Edinburgh, and Dublin Philosophical *Mag. J. Sci.* **45** 823
[50] Bao W Z, Liu D, Li P and Duan Y H 2019 Structural properties, elastic anisotropies and thermal conductivities of tetragonal LnB_2C_2 (Ln = Rare Earth) compounds from first-principles calculations *Ceram. Int.* **45** 1857
[51] Surucu G, Kaderoglu C, Deligoz E and Ozisik H 2017 Investigation of structural, electronic and anisotropic elastic properties of Ru -doped WB_2 compound by increased valence electron concentration *Mater. Chem. Phys.* **189** 90–95
[52] Ran Z, Zou C, Wei Z and Wang H 2023 VELAS: an open-source toolbox for visualization and analysis of elastic anisotropy *Comput. Phys. Commun.* **283** 108540